Chapter 1 Introduction

1.1 Overview of low temperature polysilicon (LTPS)

Polysilicon TFT is the key building block for active matrix liquid crystal display (AMLCD) and active matrix organic light emitting diode (AMOLED) due to its faster switching characteristics and high driving current. Its fabrication is similar to the conventional MOSFET process flow and the most difference is the processing temperature. The maximum temperature limited in MOSFETs is about the silicon melting-point, and the temperature in polysilicon TFT fabrication should be less than 600-650 ^{O}C, due to the commercial considerations that we can processing all fabrications on the cheaper substrate materials such as the glass or the plastic. Low-temperature-polysilicon technology is developed for this reason.

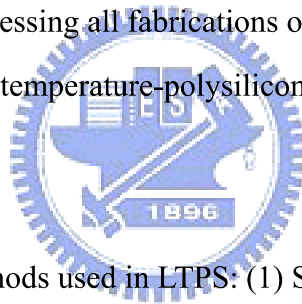

There are three main methods used in LTPS: (1) Solid-phase-crystallization (SPC), (2) metal-induced-crystallization (3) Laser-crystallization (LC):

(1) Solid phase crystallization (SPC):

The most direct method to obtain polysilicon films is heat the amorphous silicon films in a furnace. Amorphous silicon is a thermodynamically metastable phase. When the silicon film obtains a sufficient energy to overcome the initial energy barrier, the amorphous silicon starts to transfer to polysolicon. The SPC could be accomplished in a wide temperature process window corresponding to annealing times. The relation between annealing temperature and annealing time is not unique[1], since the microstructural details of the precursor-Si film play a important rule. With different deposition method and conditions[2.3], the nucleation rate would be strongly influenced. By increasing the deposition rate and the decreasing the temperature, the silicon film will form a violent structural disorder that induces the silicon hard to nucleation. Figure 1.1 (a) shows a partial RTA region method by a thin film

heater without doing damage to the glass substrate[4]. The electric characteristics is illustrated in figure 1.1 (b) and (c).

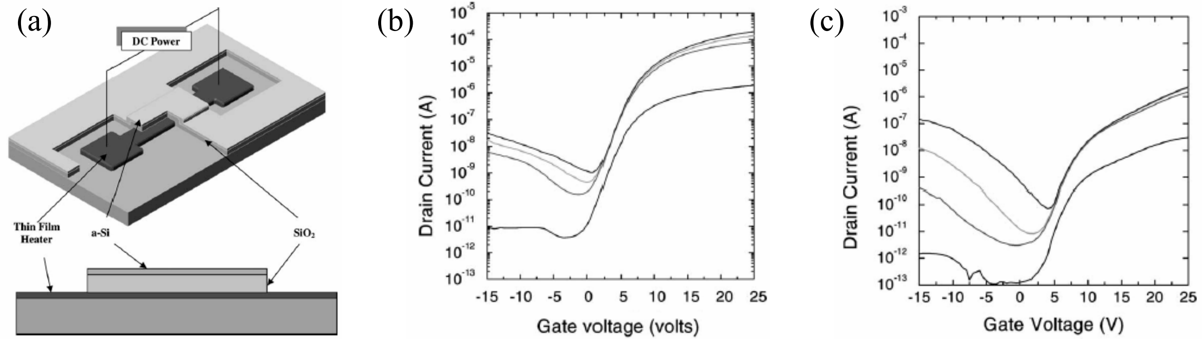

Figure 1.1 (a) Schematic diagram of solid phase crystallization of α-Si by thin film heater. (b) I-V curve of TFT by thin film heater. (c) I-V curve of TFT for furnace annealing 600°C, 20h.

(2) Metal induced lateral crystallization (MILC):

In MILC, the enhancement in grain growth is attributed to an interaction of the free electrons if the metal with covalent silicon bonds at the growing interface. MILC makes the amorphous crystallized in a lower temperature than that of SPC. At first, a nickel film was deposited on the amorphous silicon, with the increasing the temperature, the silicon and nickel combined to the formation of NiSi and $NiSi_2$, and at the temperature in the range of 450-700°C the NiSi transforms into thermodynamically favored phase, $NiSi_2$. The disilicide $NiSi_2$ is cubic with the CaF_2 structure and has a very close lattice constant match to c-Si. The nickel is the dominant diffusion species in NiSi and $NiSi_2$ such that the nickel diffused and left the silicon in a polysilicon phase. The diffusion of the nickel induced a lateral crystallization. As the result of such growth mechanism, silicide-mediated polysilicon films demonstrate a fibrous microstructure, with each fiber attributed to c-Si growth from an individual disilicide precipitate. An important problem in MILC is that there is still some residual nickel in the MILC region. MILC also has been combined with laser crystallization technology[5]. Figure 1.2 (a) is the structure and fabrication process of combining MILC and ELA[6]. Figure 1.2(b) and (c) are SEM images with different laser intensity.

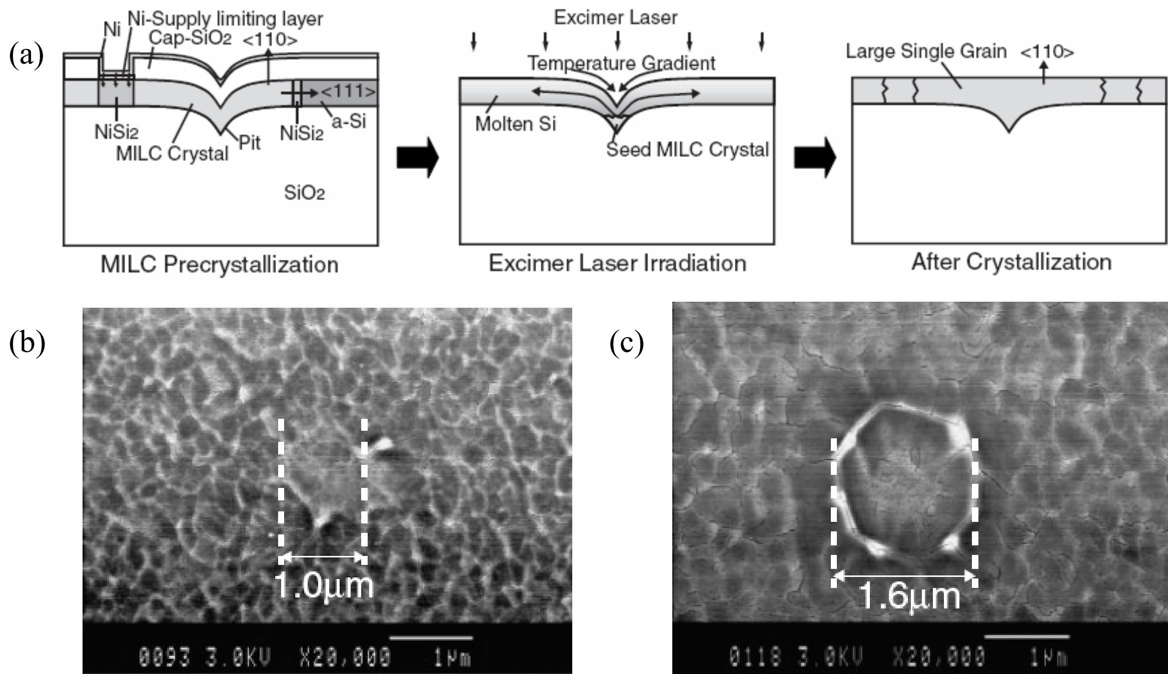

Figure 1.2 (a) fabrication procedure combining MILC and ELA with a pit structure (b) SEM image with laser energy = 733mJ/cm^2 (c) SEM image with laser energy = 775 mJ/cm^2.

(3) Laser crystallization (LC):

By using a laser, the silicon film could be heated in a certain section expected, and the substrate temperature can also be controlled less than the deformation threshold even on a plastic substrate with a thicker SiO_2 insulator layer. As the silicon film absorbs the laser light, the high laser energy not only heats the film to the melting temperature but transfer the extra-energy to the latent heat of the silicon to melting the film. Several nanoseconds later, the melted silicon film releases the energy into the substrate. At the same tine liquid-phase silicon solidifies and transfers into the polysilicon. The microscopic structure of the laser-crystallized poly-Si films depends on a variety of parameters such as film thickness, laser energy density, and laser wavelength.

By SEM measurements, it could be found that the average grain size is strongly affected by the laser energy density used for the crystallization. At the low laser energy density, the average grain size increases with increasing laser intensity. This energy regme is known as the partial melting fluence. In this laser intensity regime, the average grain size is

confined due to the large number of the nuclei and the low energy. At the high laser fluence, the average grain size is not proportional to the laser energy. This energy range is referred to as the complete melting fluence. In such regime, there is a supercooling governing the solidification of silicon. When the supercooling occurs, a great number of nuclei appear in the film such that the average grain size decreases to about 0.1μm dramatically. Between above two regimes, the third laser fluence is called as super lateral growth (SLG) regime. When the laser energy density just reaches the intense to completely melt the silicon film, there are only a few discontinuous and non-melted residual silicon islands existing in the bottom of the film, and the grain grow from the nuclei. The solid-liquid phase moves laterally in the film, and the average grain size about several times the film thickness could be obtained. However, the process window of SLG is too narrow to control precisely. If laser intensity shifts, the crystallized polysilicon film will not keep in the SLG regime but transfer to the others. The crystallization phenomenon of three regimes we mentioned above is shown in figure.1.1, and the relation between the laser fluence and the grain size is shown in figure.1.4.

(a)

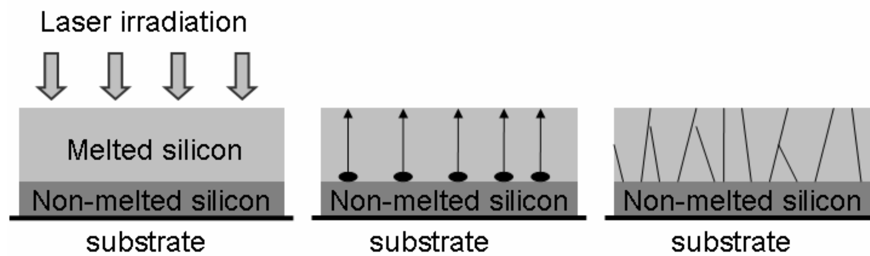

(b)

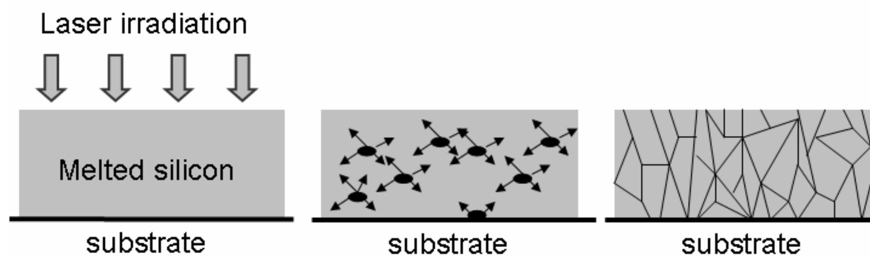

(c)

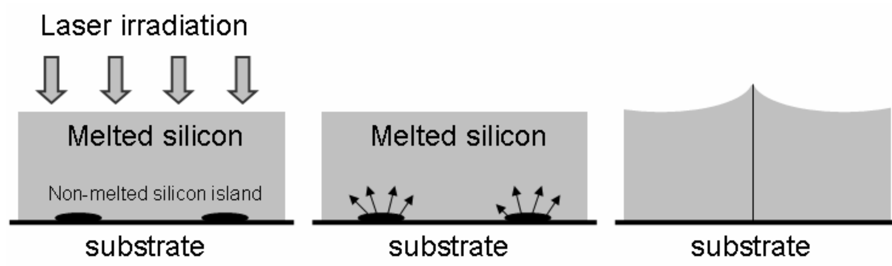

Figure.1.3 According to the laser energy fluence, the crystallization could be discussed into three regimes: (a) partially melting fluence, (b) completely melting fluence, (c) super lateral growth (SLG).

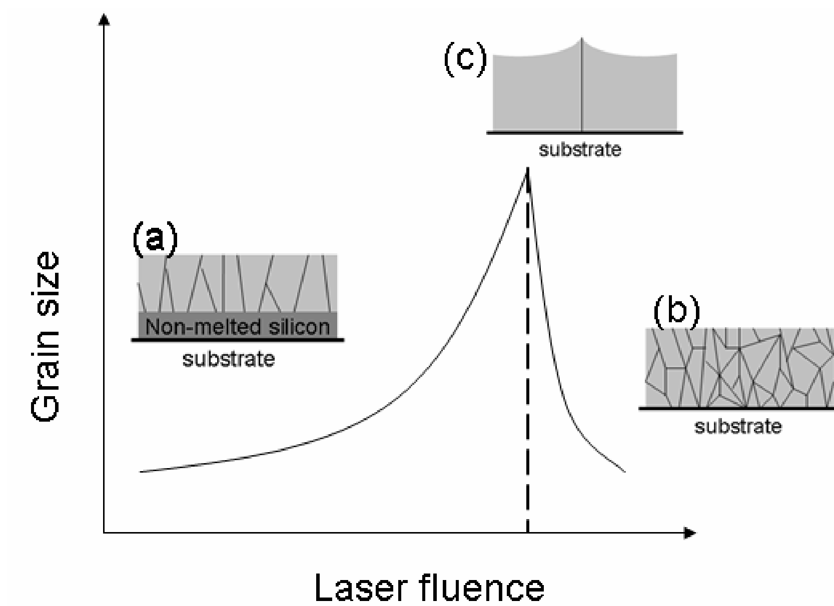

Figure.1.4 The relation between the laser fluence and the grain size.

1.2 Introduction of laser lateral crystallization

Many studies focused in enlarging the grain size, grain growth direction and nucleation position in order to obtain a single crystalline or single grain boundary in channel TFT. Thus, there are several methods developed to achieve this purpose, such as CW laser scanning direction inducing lateral crystallization, structure inducing lateral grain growth, phase-modulated excimer-laser crystallization (PMELC), and subsequence lateral grain solidification (SLS).

(1) CW laser scanning direction inducing lateral crystallization:

Akito Hara presented a method of which a neck-like silicon island structure shown in figure 1.5 is used to form a single nucleus in edge the channel and continue-wave laser can induce a lateral grain growth along its scanning direction[7]. To prevent the introduction of the other grains, the temperature gradient is controlled during solidification by using both a capping silicon on the neck structure and laser irradiation from the back surface through the glass substrate[8].

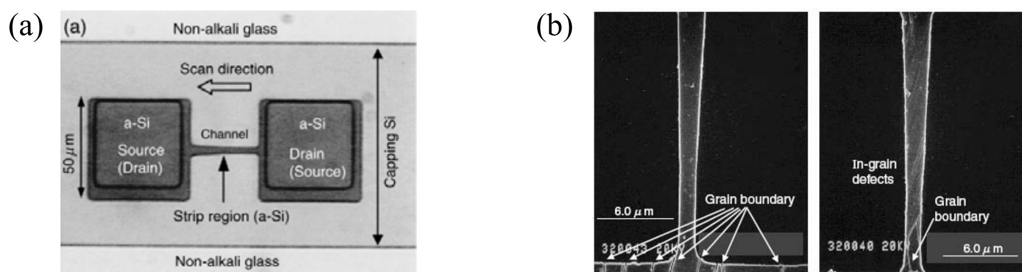

Figure.1.5 (a) A neck-like silicon island structure, (b) single crystalline in the channel (left) and single crystalline with in-grain defects (right).

(2) Structure inducing lateral grain growth

Ryoichi Ishihara presented a new approach called grain filter to control the grain size and nuclei uniformly[9,10]. The grain filter shown in figure.1.6 (a) was formed in two steps called μ-Czochealski process: First, an approximately 750-nm-thick oxide layer was grown by the thermal oxidization of a silicon wafer and subsequently patterned into grids of holes (1μm in diameter) by RIE. Then an 800-nm-thick TEOS oxide layer was deposited by PECVD to reduce the diameter of the holes to about 100nm, then a 250-nm-thick amorphous silicon film was deposited. By SEM measurements, a matrix array grain (shown in figure. 1.6 (b) and 1.4 (c)) was formed by the grain filter method. The theory of grain filter is that the amorphous silicon in the grain filter was partial melted by laser irradiation and the residual non-melted silicon formed a nucleus. And then the grain grew outward from the hole (shown in figure.1.6 (d)), a single grain would be observed by SEM.

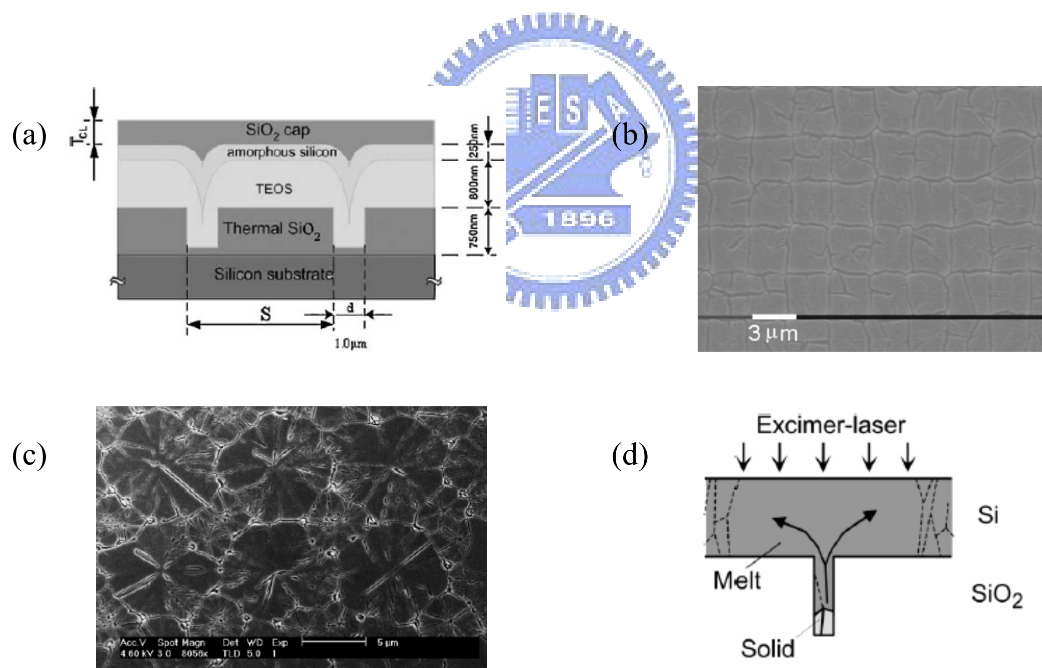

Figure.1.6 (a) the fabrication process of the grain filter, (b) and (c) matrix-array grains by the grain filter method, (d) the crystallization process in a grain filter.

The fabrication process There are still other structures designed to enlarge the grain size and controlled to achieve only one grain boundary in TFT channel, such as air bridge structure[11], heat reservoir layer[12].

(3) Phase-modulated excimer-laser crystallization (PMELC)

PMELC was mentioned and implemented in 1998 by Masakiyo Matsumura [13]. It's a novel method which changes the laser light distribution by a phase-shift mask made by quartz. Before the laser irradiation on the specimen, we insert a phase-shift mask above the silicon surface with a distance about several hundreds to thousands μm. The mask shown in figure.1.7 (a) was designed with a step on the surface to induce a laser light interference phenomenon on the silicon film surface, such that the thermal gradient formed in the silicon film would force the solid-liquid face moving along the thermal gradient direction and then the lateral grain growth occurs (shown in figure.1.7 (b)). In order to enlarging the grain size, except for changing the laser energy, distance between the sample and the mask, the step thickness on the phase-shift mask, and the pattern on the phase-shift mask to change the interference shape on the silicon film[14], combining other methods to enlarge the grain size was also studied, such as pre-depositing a thin metal film under the silicon[15] or depositing a photosensitive capping layer[16] to add the grain growth time, combining a structure design and PMELC to achieve a 2D grain growth[17,18] and a single grain in channel[19].

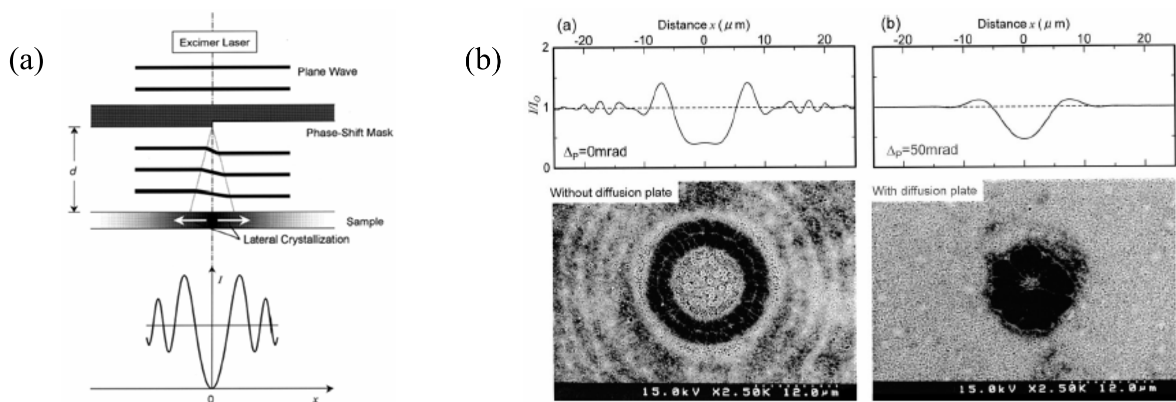

Figure.1.7 (a) Laser intensity interfered with a phase-shift mask, (b) relationship between laser intensity distribution and lateral grain growth.

(4) Subsequence lateral solidification (SLS)

SLS is a lateral crystallization method that repeats the laser pulses which could totally melt the amorphous silicon film with a constant period, and moves the specimen simultaneously, such that each laser pulse would partially overlaps with the prior one to inducing the lateral grain growth. If we use a large area laser pulse to process SLS, the lateral grain growth only happens on the edge of the laser pulse. Robert S. Sposili presented that using a mask with slits allows only a thin line-shape laser to pass the mask and irradiate on the amorphous silicon and moving the specimen perpendicular to the mask slits simultaneously induces the grain to grow in the direction of the specimen (shown in Figure.1.8 (a))[20]. By this way, we could obtain a large SLS regime. Also there are other methods to control the laser irradiation area such as shaping the laser beam to form a elliptical beam with a width of 460μm and height of 12μm by a cylindrical and a spherical lens (shown in figure 1.8 (b))[21]

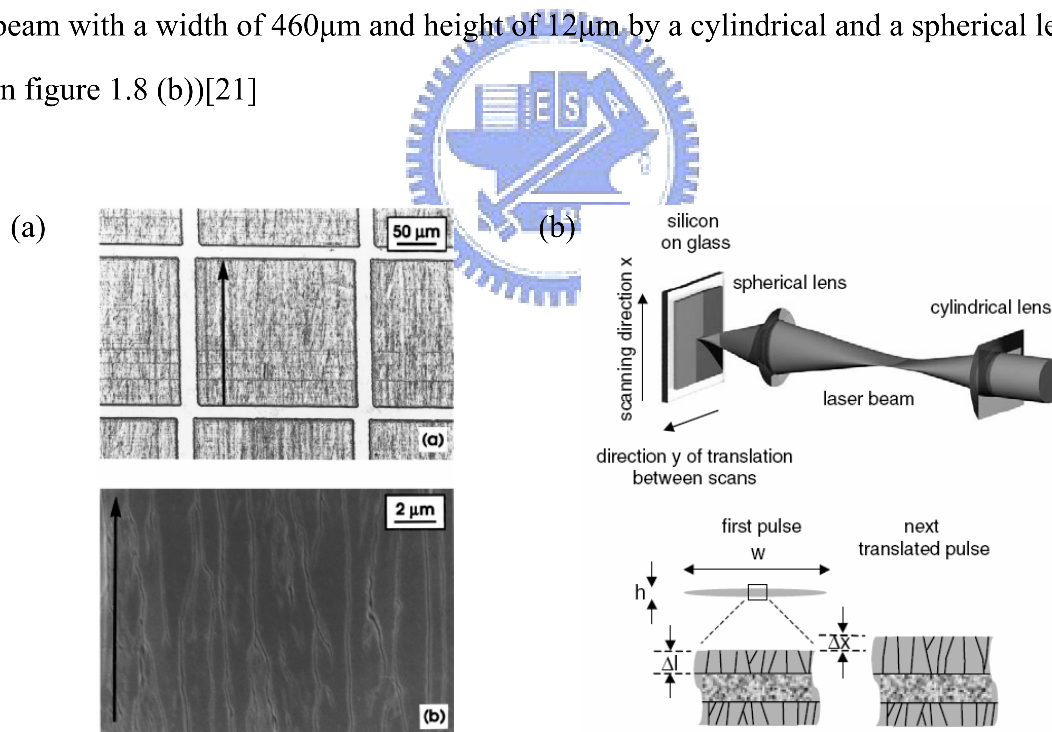

Figure.1.8 (a) the upper one is the mask pattern, the bottom picture is the SEM of the film surface after secco-etching, (b) the upper one is the laser beam modulated by spherical lens and cylindrical lens, the bottom presents the SLS process.

1.3 Motivation and thesis overview

The grain boundary in a TFT channel plays the role that decreases the electric mobility and increases the leakage current. To reducing the effect of the grain boundaries effects, lateral crystallization is studied in recently years by methods we mentioned above. In my thesis, we tried to repeat two lateral grain growth methods have been found and designed a new method to achieve a lateral grain growth purpose, and discussed about this methods' advantages or shortcomings. The final purpose in this thesis is to control the grain size, grain growth direction, and the nucleation positions precisely, such that all grain boundaries in the TFT device channel would be parallel to the channel to upgrade the device performance.

In this thesis, we divide full text into five chapters. In chapter 1, the LTPS technology and several lateral grain growth methods are mentioned and are introduced. In chapter 2, we discuss the experiment theory and make a simple heat flux simulation for the experiments we did. In chapter 3, we focused on the fabrication of our specimen, and the lateral crystallization experiments, and the results of the silicon film crystallized. In chapter 4, the polysilicon film's electrical properties would be measured by the way of four point probe measurement. In chapter 5, we would give a summary to the above results and talks about the future works.

Chapter 2 Grain growth control methods and heat flux simulation

2.1 Heat flux simulation

The software we use to simulate the laser crystallization process is FEMLAB which is a interactive environment for modeling and solving many kinds of scientific and engineering problems based on partial differential equations (PDEs). One of the tools is heat transfer simulation, and we choose the mode – transient analysis but not the steady state because we would try to analyzing the full process of the laser crystallization. We define the mesh shape to be triangle illustrated in figure 2.1, and the mesh density increasing would add our simulation time and the precision of the results simultaneously. We set each time step to be 1ns and the total simulation time to be 800ns such that we could confirm the accuracy and the completeness of the results at the same time. The following example will illustrate a simple simulation about the laser crystallization.

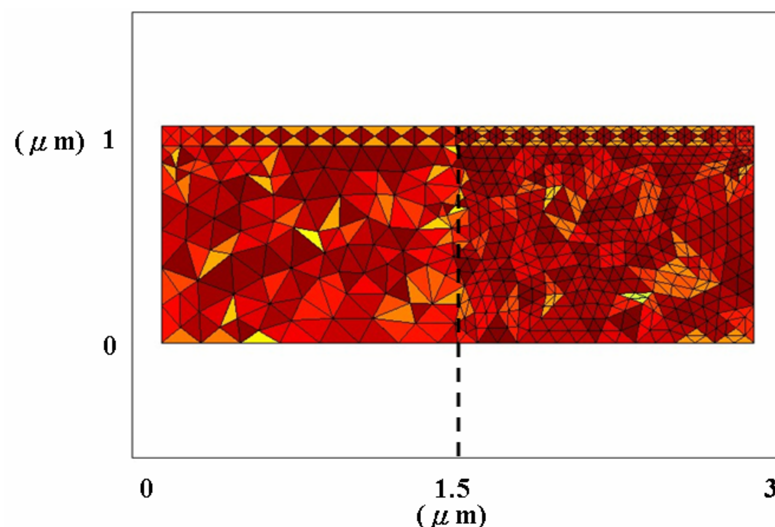

Figure 2.1 The left part of picture is the normal meshes in the structure and the right part is the refined meshes in the structure. The refine meshes would increase the accuracy of the final result.

We assume a simple structure in Figure 2.2 and the dimensions of each side is labeled. The boundary conditions are then written as

$$\left.\frac{\partial T}{\partial x}\right|_{x=0}=0, \quad \left.\frac{\partial T}{\partial x}\right|_{x=3\mu m}=0, \quad . \tag{Eq.2.1}$$

$$\left.\frac{\partial T}{\partial y}\right|_{y=1.1\mu m}=0, \quad T\big|_{y=0}=T_s=23^{\circ}C . \tag{Eq.2.2}$$

where T is the temperature and the T_s is the ambient temperature and the initial sample temperature. The initial condition is $T\big|_{t=0s}=T_s=23^{\circ}C$ for all regions. An equation at time t is $c\frac{\partial T}{\partial t}=\nabla\cdot(\kappa\nabla T)+Q$, where c and κ are specific heat and thermal conductivity, respectively. Q is the heat generation or loss rate per unit volume.

We have neglected the effects of infrared light emission and absorption, and therefore heat generation is only coursed by the absorption of the excimer laser light. The absorption coefficient, α, is a wavelength dependent value, and we measured it by n&k analyzer. It also a temperature-dependent value but its change is not essential. We used a fixed value of $0.7cm^{-1}$ for α. The part of the laser light irradiation is represented as the following equation:

$$aborption = T\times\alpha I_0(t,y)\exp(\alpha(y_0-y)) \tag{Eq.2.3}$$

where y_0 is the position at the top of the α-Si film ,I_0 is the light intensity irradiated to the sample surface and T is the transition coefficient. We have assumed that I_0 is a square-like time dependence that takes a constant value from t=0s to t=25ns. We also considered the additional heat stored and released in the silicon film during the crystallization process. We set a temperature regime from 1350 to $1440^{O}C$ for the latent heat stored in the silicon film at t<25ns (during laser irradiation) and released at t>25ns (after laser irradiation). The value of

latent heat is 3000J/cm^3 and other parameters such as specific heat, thermal conductivity…etc. were list in table 2.1[16].

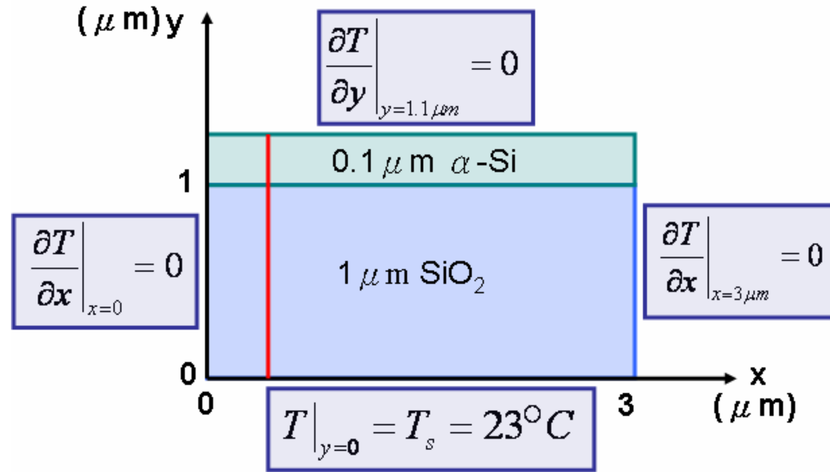

Figure 2.2 The structure for a simple simulation, the toplayer is α-Si and the bottom layer is SiO_2. The dimensions and the boundary conditions of each side are labeled on it.

Table 2.1 Thermal conductivity, specific heat and other parameters used in the simulation. The value of absorption coefficient was measured by n&k analyzer.

	Si	SiO_2
κ ($WK^{-1}m^{-1}$)	25	1.4
c ($Jm^{-3}K^{-1}$)	2.3×10^6	2.3×10^6
α (m^{-1})	7×10^{-7}	—
L (Jm^{-3})	3×10^9	—
T_m (°C)	1410	—

The simulation results includes the temperature curve of a particular point versus the time, the temperature curve of a particular line versus the time, the thermal distribution at a certain time, the contour lines of the temperature at a certain time and the heat flux at a certain time. The results we mentioned above will be illustrated in figure 2.3. From the temperature curve of a particular point versus the time we could understand the state of the silicon and from the contour lines of the temperature at a certain time and the heat flux at a certain time we could know the grain growth direction which is in the anti-direction of the heat flux. In 2.3

(b) there is no other special design, the laser energy tends to transfer to the substrate such that the grain would grow form the interface of two layers to the top surface vertically. In figure 2.3 (c) there exists a thermal platform region which represents the latent heat releasing during the liquid-phase Si transferring to solid-state Si. By analyzing figure 2.3(d) we could obtain a conclusion that after laser irradiation (at 25ns) the most energy absorbed by the α-Si layer. With the time passing, the exceeding heat transfer to the bottom SiO_2 layer and the temperature of the Si film tends to be same in each depth due to the high thermal conductivity of Si. Four results above are useful tools to analyze the crystallization process.

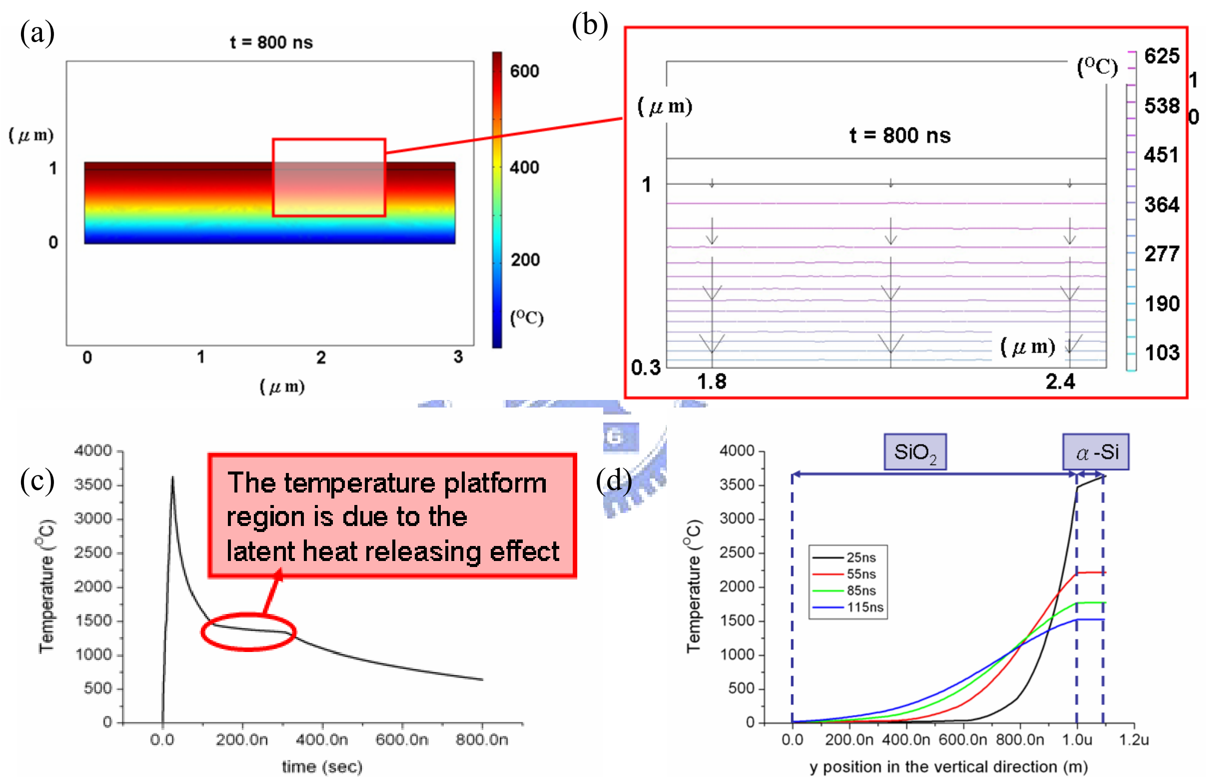

Figure 2.3 (a) Thermal distribution at a certain time = 800 ns, (b) the contour lines of the temperature and the heat flux at a certain time = 800ns (c) Temperature curve of a particular point (1.5μm, 1.1μm) versus the time (d) Temperature curve of a particular line (along the red line in figure 2.2) versus the time (at 25ns, 55ns, 85ns and 115ns)

2.2 Lateral crystallization induced by the metal reflection layer

A lateral grain growth controlled by the metal reflection layer was presented in 2001 by Min-Koo Han[22]. The metal Al was chosen to be the reflection layer capping on the α-Si. The TEM image and the ELA process diagram are shown in Figure 2.4.

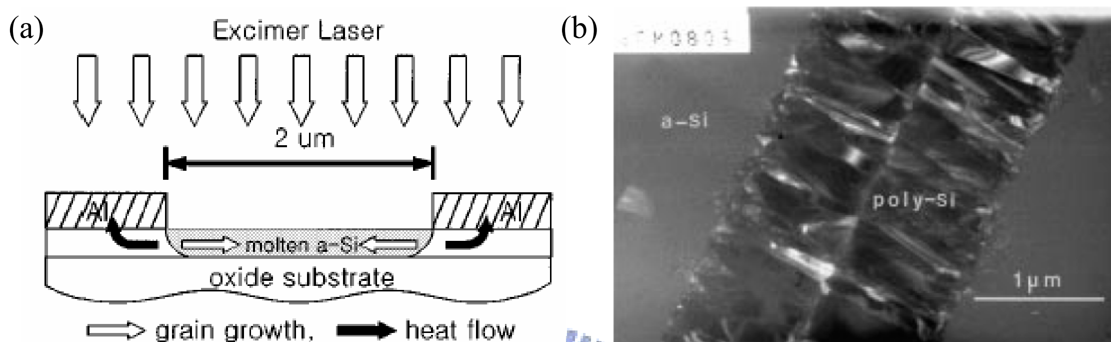

Figure 2.4 (a) ELA process diagram. (b) TEM image of the poly-Si film recrystallized by ELA process.

The structure of this method is illustrated in Figure 2.5. All films were deposited on a glass substrate which could endure high temperature about 500°C. the buffer layer was consisted of 50nm SiN_X and 100nm SiO_2. The SiN_X and SiO_2 films could prevent the diffusion of the impurity from the glass substrate to the amorphous silicon film and decrease the heat flux diffusion rate from the amorphous silicon layer to the substrate due to their high thermal conductivity. Furthermore, quality of the α-Si film deposited on the glass substrate directly is not well enough, and with the buffer layer the film quality could be controlled as well as we expected. The metal layer we chose is Cr that deposited on the α-Si film. The purpose of this layer was to be the metal reflection layer which would block the laser light and be treated as the heat sink layer due to its high thermal conductivity during the laser irradiation process such that we could selectively melt the silicon film. The silicon under the shielded metal could receive less energy than that without shielded metal, and the energy was not enough to melt the silicon, so the silicon remained the solid-phase. The silicon irradiated

by the laser directly was heated to a high temperature more than the melting temperature and transferred to a liquid-phase. The solid-phase silicon near the edge of metal pattern became nuclei during the laser irradiation process, and the grain grew from the nuclei to the liquid silicon region. The lateral grain growth could be observed at the edge of the metal pattern.

Compared with a conventional ELA process, we could obtain a lateral grain growth by the metal reflection layer method. It could be expected to obtain a larger grain growth size at the same laser energy regime, the well-arranged growth direction which is perpendicular to the edge of the metal pattern and the precise grain growth position.

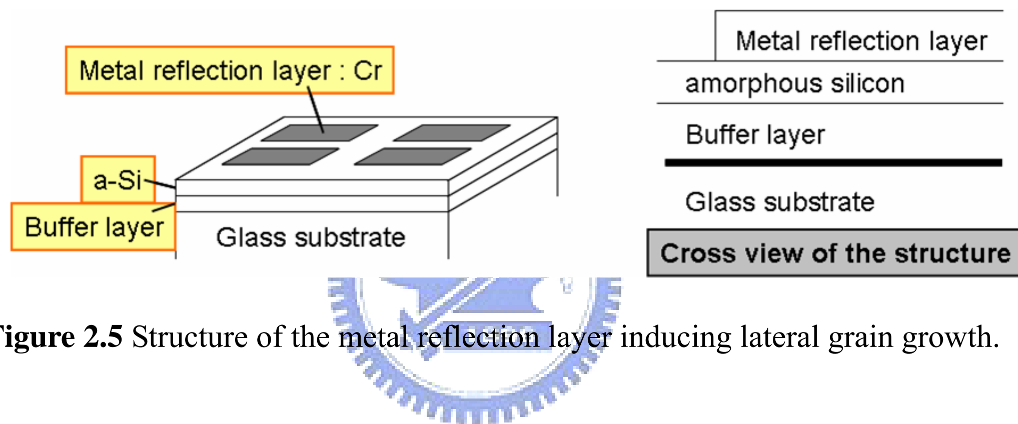

Figure 2.5 Structure of the metal reflection layer inducing lateral grain growth.

During the ELA process, the laser light was absorbed by the silicon film and released again. By simulating the heat flux transferring, we could analyze the temperature distribution in our structure. The temperature gradient in the water-level direction of the silicon film forms the lateral grain growth.

Thus the structure shown in figure 2.5 would be simulated to analyze the thermal distribution at different time step. The simulation structure is that a buffer layer consisted 50nm SiN_X and 100nm SiO_2 was deposited on a glass substrate by PECVD and following the 50nm α-Si was deposited on the buffer layer by PECVD. The 100nm Cr film was deposited on the α-Si by e-gun evaporator and patterned into the island shape by photolithography. The structure was shown in figure 2.6.

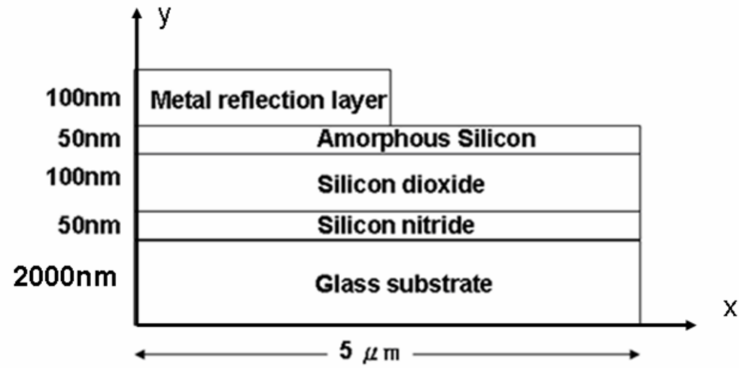

Figure 2.6 Simulation structure of the metal reflection layer method.

When the laser irradiation intensity is 300mJ/cm^2 the temperature distribution at the top of the Si film is shown in figure 2.7. The region x<2.5μm is the sample with metal capping layer, it could be expect that the α-Si under the metal didn't reach the melting point due to the shield effect of the metal. The temperature curve of the silicon with and without capping metal is shown in figure 2.8. By comparing two diagrams, we could find that the silicon film covered by the metal couldn't reach the melting temperature during the ELA process. In the figure 2.9 (a), the temperature distribution in our each layer of our simulation structure was shown in it .In 2.9 (b), the contour lines and heat flux was shown in it by color lines and the arrows such that we could analyze the heat transfer and the grain growth direction during ELC process.

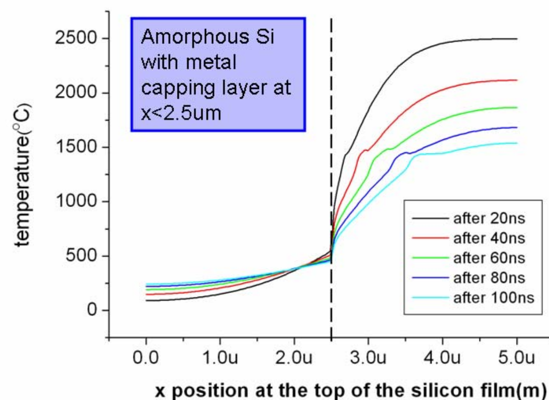

Figure 2.7 Temperature distribution at the top of the silicon film at each time step.

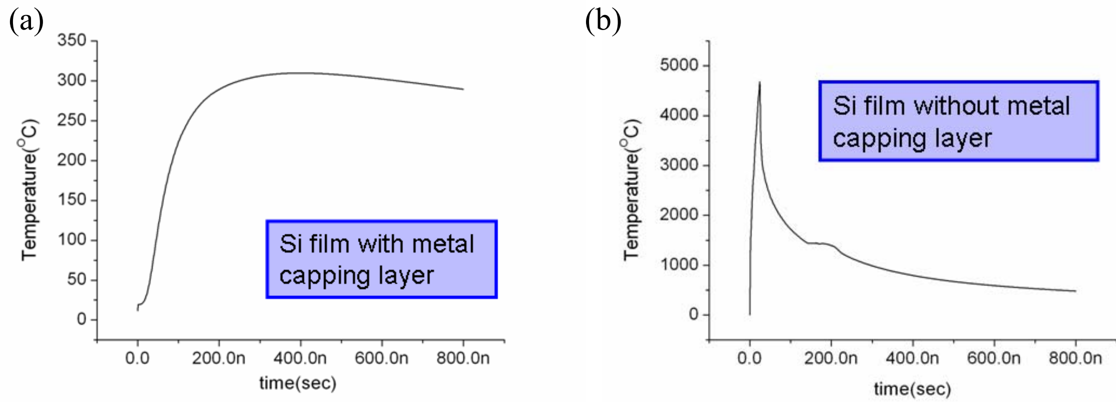

Figure 2.8 Temperature curve versus time after laser irradiation for the silicon film (a) with metal capping layer and (b) without metal capping layer.

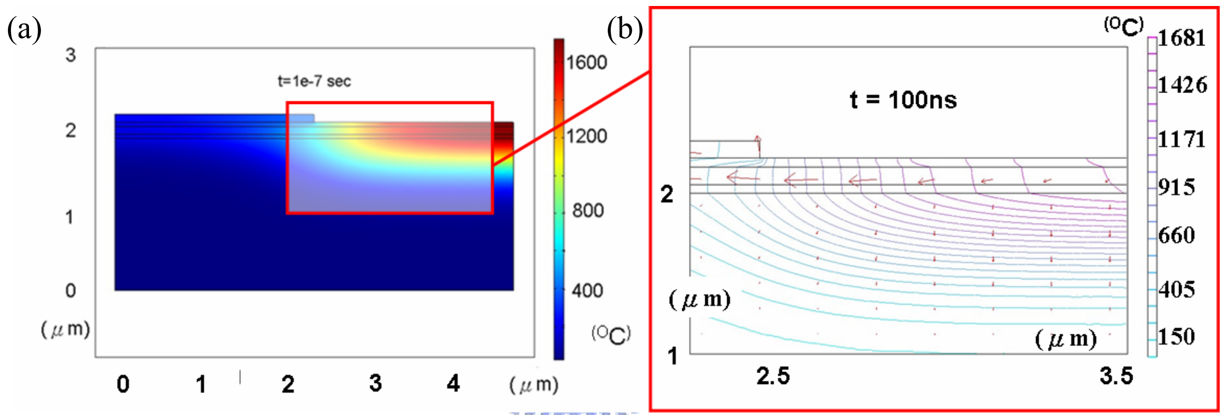

Figure 2.9 (a) Thermal distribution in the full structure region mentioned at t = 100ns, (b) the color lines are contour lines of the temperature and arrows represent the heat flux distribution at t = 100ns.

2.3 Nucleation positions controlled by "nano-holes"

A method that controls the grain growth direction by a recessed-channel structure (shown in figure 2.10) was presented in 2001 by Huang-Chun Chen[24]. The laser energy was well controlled to be in the range which could totally melt the thin α-Si region and partially melt the thick α-Si region. The laser energy is not large enough to melt the thicker α-Si film such that the unmelting Si was treated as crystallization nuclei and the grain growth forms those nuclei to the thin Si film region. The grain boundary forms in the middle of the channel region, the SEM image is shown in Figure2.11.

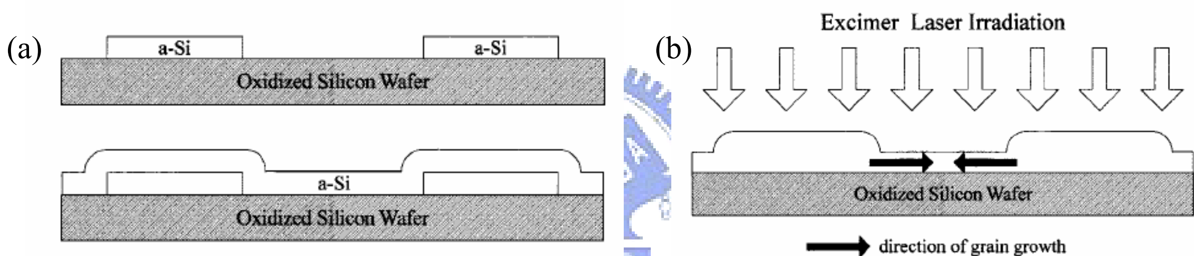

Figure 2.10 (a) the fabrication process of the recessed-channel structure (b) grain growth direction after the laser irradiation.

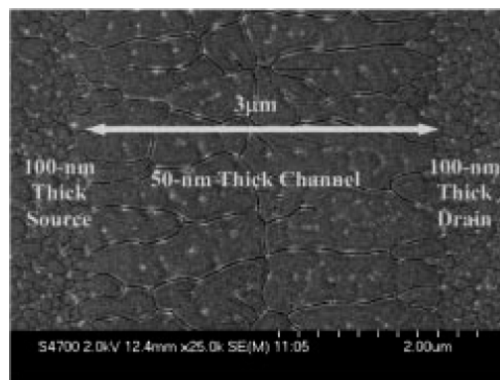

Figure 2.11 SEM image of channel region and an obvious grain boundary existed in the middle of channel region.

The nano-hole structure and the whole crystallization process are shown in figure 2.12. In this structure, the silicon film was thicker at the edge of the holes due to the partial Si deposited on the sidewall of the hole. During the laser irradiation, the Si film at the edge of the nano-holes was partially melting and the nuclei were well controlled in the edge of the holes. Furthermore, the silicon has a higher thermal conductivity than SiO_2 and the heat flux would not transfer to the substrate by passing the SiO_2 layer but through the Si on the sidewall of the holes. With this structure, a lateral grain growth starts form the Si film at the edge of the holes to the other outside region until the grains collided with others.

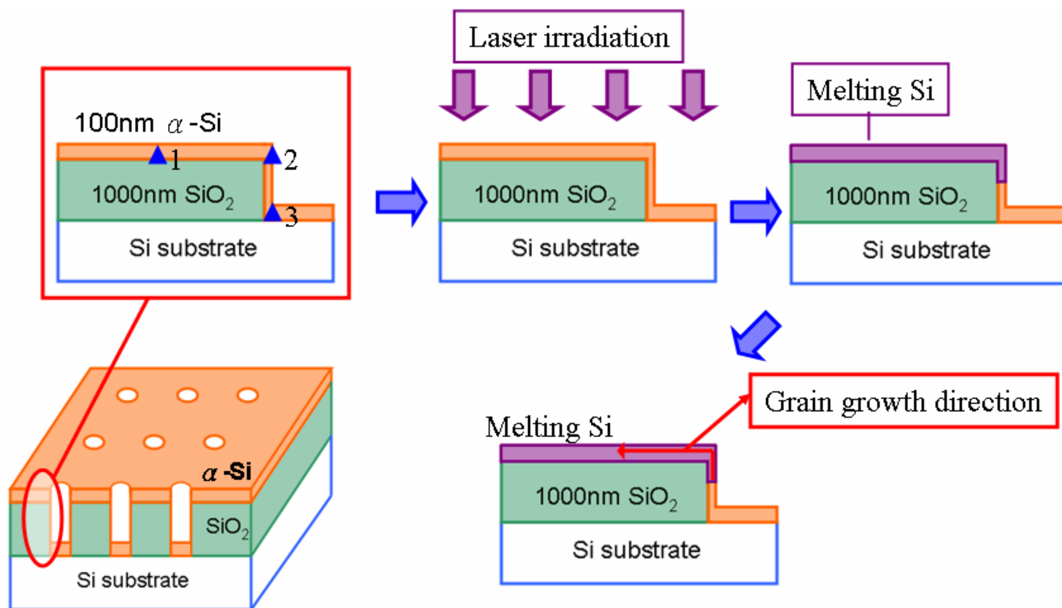

Figure 2.12 Nano-hole structure, cross view of a single nano-hole and the whole crystallization process.

Input laser intensity is $300mJ/cm^2$, we compare temperature versus time in figure 2.13 at three points in figure 2.12. It shows that the temperature of the silicon at the bottom of the silicon film couldn’t reach the melting temperature during the crystallization process. At the point 2, because partial laser energy was transferred to the under silicon layer at the sidewall the maximum temperature was less than that of point 1. The thermal distribution is illustrated in figure 2.14 (a) at t = 200ns. By analyzing he thermal distribution along the sidewall of the hole (shown in figure 2.15), we could find the melting depth of the silicon film which is about

3000Å. The nuclei formed at the interface between the melting and unmelting region, and the grains grew from those nuclei outward to the region around the hole. The grains stopped until colliding to other grains. In figure 2.14 (b), the arrows indicate heat flux in α-Si near the hole was parallel to the interface between the silicon film and buffer oxide layer and this phenomenon would tend to forms the lateral grain growth.

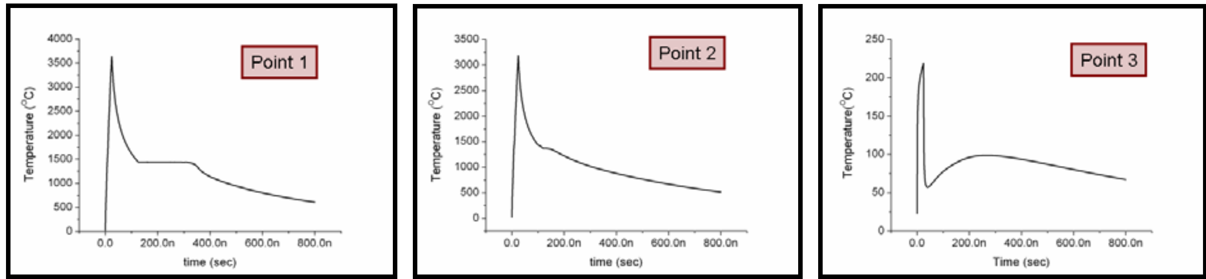

Figure 2.13 The curve of temperature versus time at each point shown in figure 2.12.

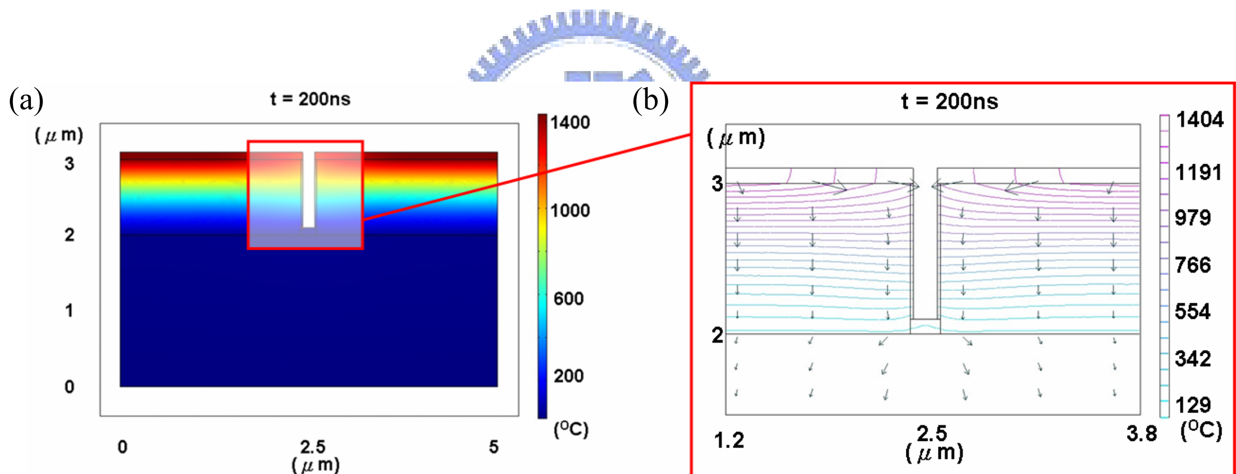

Figure 2.14 .(a) Thermal distribution in the full simulation structure region at t = 200ns, (b) Color lines are contour lines of the temperature and arrows represent the heat flux distribution at t = 200ns (fine view).

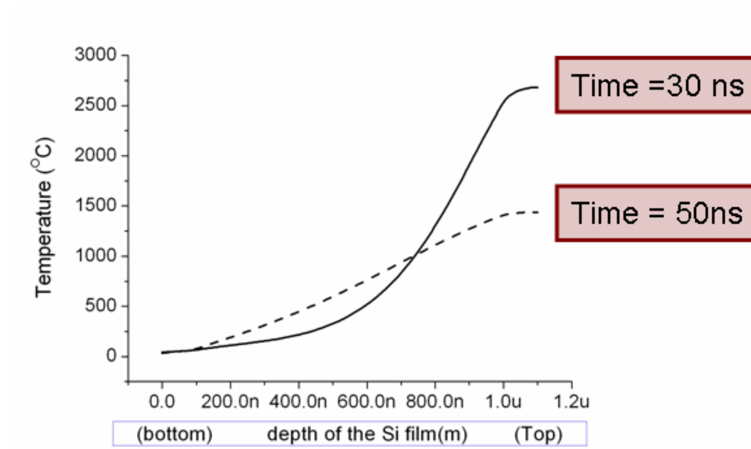

Figure 2.15 The curve of temperature along the sidewall of the hole at time = 30 ns and t = 50 ns.

2.4 Lateral grain growth induced by laser intensity distribution modulation with single slit diffraction

A phase modulated excimer laser crystallization (PMELC) method[13] we mentioned before could control the light intensity distribution well. By controlling the light intensity distribution we could control the thermal distribution at the same time. In figure 2.16, we assumed I_1 is the laser intensity at which the lateral grain growth begins and I_2 is the laser intensity that is the end of the lateral grain growth. Changing the distance between the mask and the sample would change the intensity distribution along x-axis and try to control the grain growth length. A single slit diffraction method would forms a similar intensity distribution to PMELC. As light through a single slit, a light diffraction phenomenon appears at the screen with a proper distance from the slit. In figure 2.17, the intensity distribution is a function of the slit width, the light wavelength, the distance between the slit and the sample and the position far from the center position.

$$I = I_0 \cdot \left(\frac{\sin^2(\beta)}{(\beta)^2}\right) , \qquad \text{where } \beta = \frac{\pi a \sin\theta}{\lambda}, \qquad \text{(Eq.2.4)}$$

The laser intensity = 0 at the position $\beta = m\pi$, m = 1, 2, 3 …, such that

$$\frac{\pi a \sin\theta}{\lambda} = \pm m\pi , \qquad \text{and} \quad \sin\theta_m = \pm {m\lambda}/{a}. \qquad \text{(Eq.2.5)}$$

To simplify the calculation, we assume that $\sin\theta = \frac{y}{L}$ and the center diffraction region width on the sample is $y = {2\lambda L}/{a}$. By tuning the distance between the sample and the mask, we could control the center region to change the slope of the intensity versus y position. With a proper slope the lateral grain growth length could be controlled to a maximum value.

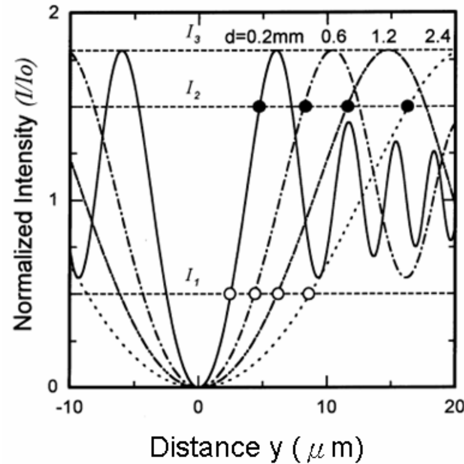

Figure 2.16 Distribution of the laser intensity with different distance between the mask and the sample

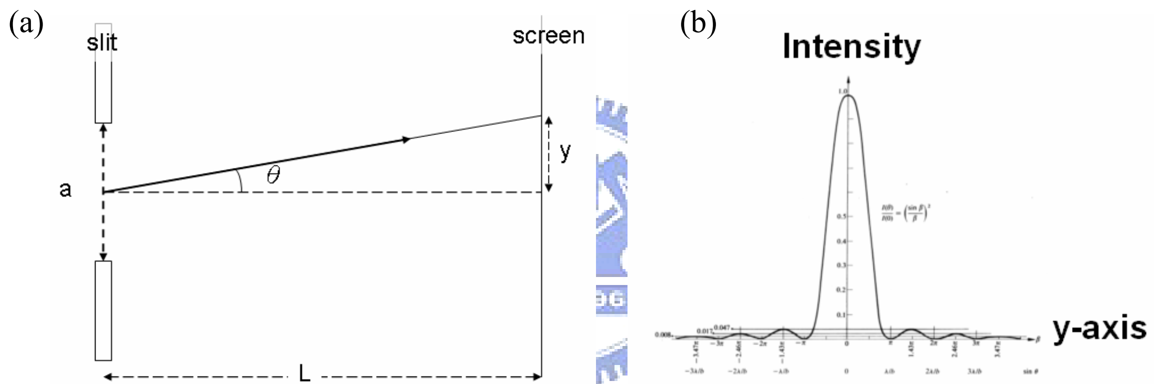

Figure 2.17 (a) Single slit diffraction structure. (b) Intensity versus position on the screen along y-axis.

However, when the distance between the slit and the screen is too small (it means the ratio of $\frac{L}{a}$ is not large enough), the intensity distribution would not be the shape like figure 2.17 (b). The diffraction effect still exists and the intensity distribution is like the shape as Figure 2.18[25]. This phenomenon means that with the slit approaching to the sample original single slit diffraction – Fraunhofer diffraction (far field diffraction) transfers to Fresnel diffraction (near field diffraction).

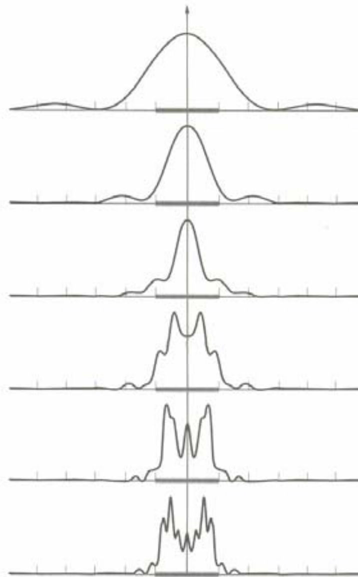

Figure 2.18 A succession of diffraction patterns at increasing distance form a single slit; Fresnel at the bottom (nearby diffraction), going toward Fraunhofer at the top (faraway diffraction).

We introduce the laser intensity distribution into the simulation. The structure (shown in figure 2.19) is that the 700nm SiO_2 film on the silicon substrate and the 100nm α-Si was deposited. There is a mask arranged above the sample such that the laser light would pass through a single slit before the laser irradiates on the sample, and the laser intensity distribution would forms in the shape we expected.

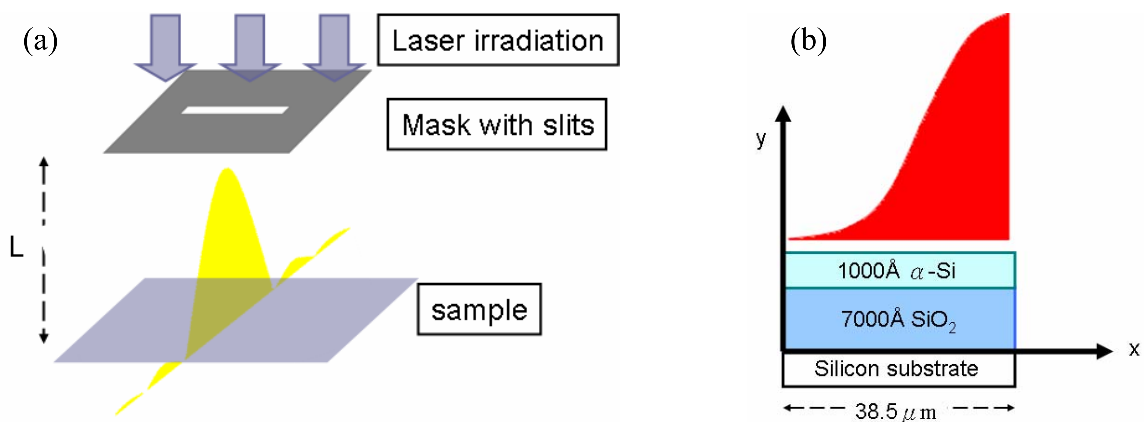

Figure 2.19 (a) The single slit optical instrument and (b) the sample structure with the intensity distribution for the simulation.

Figure 2.20 (a) is the thermal distribution at t = 100 ns by the single slit method. We could find that after the laser irradiation the thermal distribution is similar to the laser intensity distribution (we only show only 10μm length in x direction of our structure). The heat flux arrows (figure 2.20 (b)) indicate that the grains grew from the low temperature region to the center high temperature region. At the region 26 to 27μm, the lateral heat flux phenomenon is obvious dramatically. That's the lateral grain growth region and later we'll combine the results of the simulation and the experiment results in chapter 3 to confirm our simulation results.

In figure 2.21, the temperature distribution curve shows that after irradiation (the black line) the thermal distribution is similar to the initial laser intensity distribution. At the position of 20μm the temperature curve versus time is illustrated in figure 2.22 (a) and that at the position of 30μm is illustrated in (b). We could find that at 20μm the laser energy seems couldn't totally melting the silicon film such that the temperature stops at the temperature which we assume that's the solid-liquid state temperature and at 30μm the laser energy could completely melt the silicon film and the exceeding energy heats the liquid-state silicon film. The lateral grain growth occurs between the two conditions because when the energy didn't reach the value to melt the full silicon film, the heat flux tends to transfer to unmelting Si under the melting Si such that the grain would grow form this unmelting Si to the totally melting region.

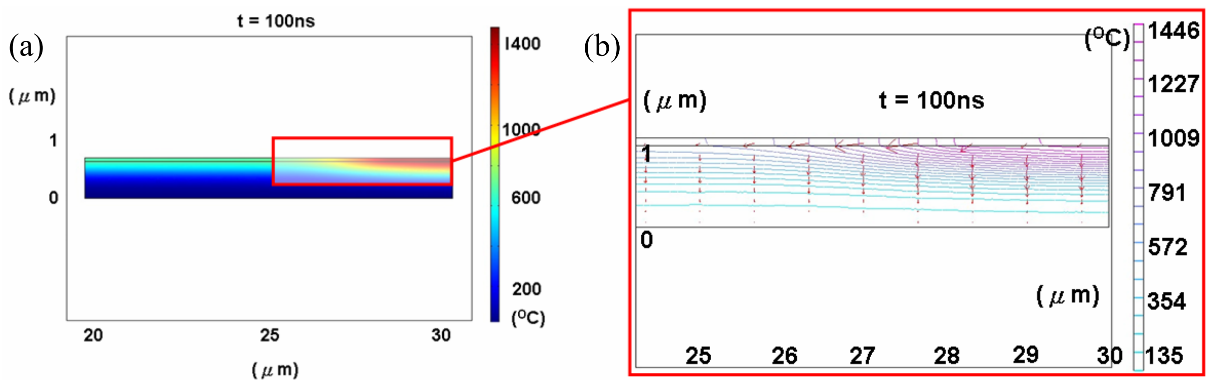

Figure 2.20 (a) The thermal distribution in the full structure region mentioned at t = 100ns, (b) The contour line of the temperature and the heat flux distribution at t = 100ns.

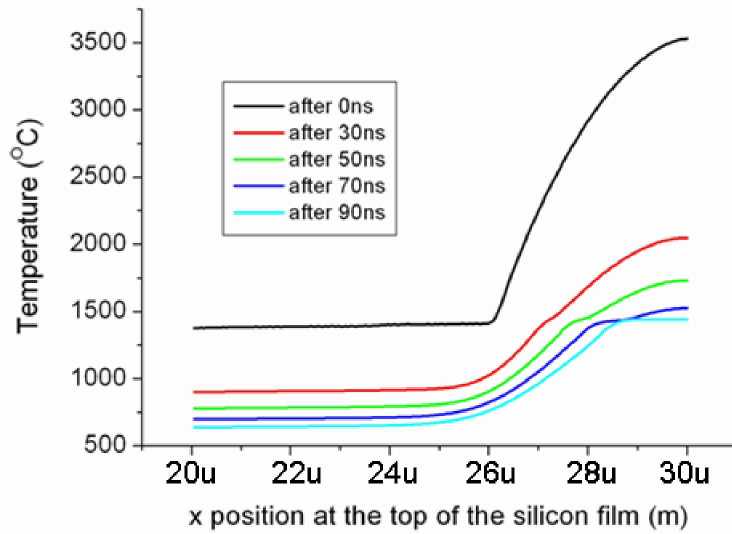

Figure 2.21 The temperature distribution on the top of the silicon film after the laser irradiation 0 ns, 30ns, 50ns, 70ns and 90ns.

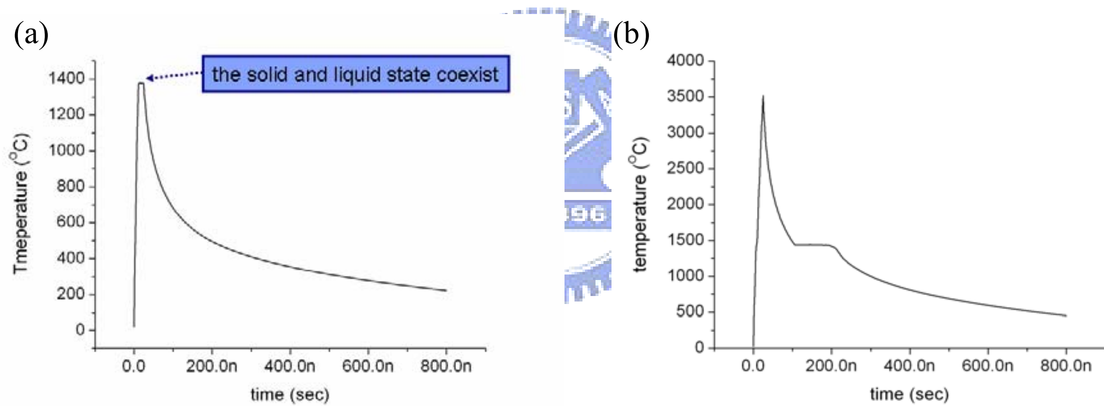

Figure 2.22 The temperature curve versus time at (a) the x-position = 20μm and (b) the x-position = 30μm.